Multiphase guaiacol photooxidation: Fenton reactions, brown carbon, and secondary organic aerosol formation in suspended aerosol particles

David O. De Haan,[1] Lelia N. Hawkins,[2] Jacob A. Weber, [2] Benjamin T. Moul, [2] Samson Hui, [1] Santeh A. Cox, [1] Jennifer U. Esse, [1] Nathan R. Skochdopole, [1] Carys P. Lynch,[1] Chen Le,[1] Mathieu Cazaunau, [3] Antonin Bergé, [4] Edouard Pangui, [3] Johannes Heuser, [3] Jean-François Doussin, [3] Bénédicte Picquet-Varrault[3]

[1] Department of Chemistry and Biochemistry, University of San Diego, 5998 Alcala Park, San Diego CA 92110 USA

[2] Hixon Center for Climate and the Environment, Harvey Mudd College, 301 Platt Blvd, Claremont CA 91711 USA

[3] Université Paris-Est Créteil and Université Paris Cité, CNRS, LISA, F-94010 Créteil, France

[4] Université Paris Cité and Université Paris-Est Créteil, CNRS, LISA, F-75013 Paris, France

KEYWORDS. Multiphase, smoke plume, photobrowning, photosensitizer, photobleaching, surface enhanced, Fenton.

ABSTRACT

Guaiacol, present in wood smoke, readily forms secondary organic aerosol (SOA), and, in the aqueous phase, brown carbon (BrC) species. Here, BrC is produced in an illuminated chamber containing guaiacol(g), HOOH(g) as an OH radical source, and either deliquesced salt particles or guaiacol SOA at 50% relative humidity. BrC production slows without an OH source (HOOH), likely due to low levels of radical generation by photosensitization, perhaps involving surface-adsorbed guaiacol and dissolved oxygen. With or without HOOH, BrC mass absorption coefficients at 365 nm generated by the guaiacol + OH reaction reach a maximum at ~6 h of atmospheric OH exposure, after which photobleaching becomes dominant. In the presence of soluble iron but no HOOH, more BrC is produced, likely due to insoluble polymer production observed in previous studies. However, with both soluble iron and HOOH (enabling Fenton chemistry), significantly less SOA and BrC are produced due to very high oxidation rates, and the average SOA carbon oxidation state reaches 2, indicating carboxylate products like oxalate. These results indicate that SOA and BrC formation by guaiacol photooxidation can take place over a wider range of atmospheric conditions than previously thought, and that the effects of iron(II) depend on HOOH. Multiphase guaiacol photooxidation likely makes a significant contribution to producing highly oxidized SOA material in smoke plumes.

Synopsis: Guaiacol reacts in aerosol particles and water droplets, contributing to increasing brownness in fresh smoke plumes. Dissolved iron increases the amount of brown material formed, unless HOOH is also present.

Introduction

Guaiacol and catechol are two of the most abundant phenolic species emitted during biomass burning.[1, 2] Guaiacol (or *o*-methoxyphenol) accounts for almost 2% of the total gas and particulate non-methane emissions from burning pine wood.[2] Although emitted almost entirely into the gas phase,[2] guaiacol forms secondary organic aerosol (SOA) efficiently during dry photooxidation, with measured SOA yields as high as 54%,[1, 3] and accounts for approximately 16% of total SOA formation in a dry smoke plume.[4] It forms hydroxylated, ring-opened, and ring-fragmented acid, anhydride, and lactone aerosol products with a high average O/C ratio of 0.9 and an average carbon oxidation state (OS_C) of +0.5.[1]

Guaiacol is also taken up into aqueous phase aerosol and cloud droplets in the atmosphere, where its oxidation forms both SOA[3] and light-absorbing, oligomeric organic species known as brown carbon (BrC).[5] SOA formed in the aqueous phase (aqSOA) can reach yields of nearly 100% in the presence of common photosensitizers that form triplet carbon ($^3C^*$) excited state species.[6] In photooxidation experiments using OH radicals photolyzed from HOOH, slightly higher O/C ratios of 0.85 to 1.23 can be reached in the bulk aqueous phase[7, 8] than in dry experiments,[1] even though significantly more of the guaiacol precursor was used up in dry experiments with similar average OS_C levels. In addition, many dimers, trimers, and oligomer products are detected in aqueous-phase guaiacol oxidation experiments.[8, 9] These conjugated oligomers are the major BrC species in low-NOx experiments. Direct photolysis of guaiacol and of structurally similar compounds like vanillin in the absence of an OH source can also produce aqSOA, although the products are not as oxidized and are not formed as efficiently as when using HOOH as an OH source.[7, 10] If guaiacol SOA produced under dry conditions is dissolved in water and subsequently photolyzed, however, no loss of average molecular mass was observed, along with little photobleaching.[11] In the presence

of high levels of NOx, nitroguaiacol species are the major oxidation product[12, 13] and contribute strongly to BrC light absorption in the aqueous phase.[14]

Several groups have explored dark reactions between Fe^{3+} and guaiacol in the absence of oxidant precursors.[15-17] Under acidic conditions, these reactions rapidly produce insoluble "poly-guaiacol" and soluble oligomers that are strongly light absorbing[15] and have rather low oxidation states (OS_C = -0.30).[16] These dark reactions are slowed only slightly by diacids complexing iron.[17] The atmospheric significance of these dark reactions remains unclear, however, since soluble iron also reacts in the dark with HOOH, generating OH radicals by the Fenton reaction. Under solar irradiation, the photo-Fenton reaction between soluble iron and HOOH typically generates even more oxidizing conditions than does oxidation by aqueous OH,[18] but the reactivity of guaiacol with soluble iron in the context of oxidative Fenton and photo-Fenton reactions has not been studied.

With just a few exceptions,[19] nearly all published studies of aqSOA formation by guaiacol and its associated BrC formation and photobleaching have been performed in bulk aqueous solutions, rather than in suspended aqueous aerosol particles or droplets. Because of this, little is known about the importance of multiphase, liquid surface, and/or organic aerosol phase processes in the aqueous oxidation of methoxyphenol species like guaiacol. Here, we report cloud chamber measurements of guaiacol interacting with aqueous phase droplets under low-NOx conditions with simulated sunlight, OH photooxidation, Fenton cycling, and photo-Fenton cycling. We find that SOA and BrC formation by guaiacol photooxidation can occur in deliquesced seed particles but also at moderate RH levels (50%), and that BrC photobleaching begins after the equivalent of 6h of atmospheric OH exposure. Soluble iron(II) generates additional BrC in the absence of HOOH, but destroys SOA and BrC in the presence of HOOH due to rapid oxidation via Fenton chemistry.

Materials and Methods

CESAM (French acronym of Chamber for Experimental Multiphase Atmospheric Simulation) is a 4.2 m^3 temperature-controlled cloud chamber whose pressure is kept slightly above ambient with inlet flows of 20% high purity oxygen and 80% nitrogen from an LN2 tank, as described earlier.[20] Na_2SO_4 seed particles were generated from a 10 mM solution made with ultrapure water (18 MΩ·cm) using an atomizer (TSI 3076) and added to the chamber through a diffusion dryer. In some experiments, soluble iron-containing seed particles were generated from a 10 mM Na_2SO_4 / 0.31 mM $FeSO_4$ solution. The pH of both types of atomizer solutions was neutral (pH = 6 to 7). Butanol-*d9* (EurIsotope, 25 ppb final gas conc.), used as an OH tracer, and guaiacol gas were added to the chamber by flushing inlet nitrogen through a glass bulb containing measured amounts of the given pure liquid. Three 6500 W Xe arc lamps shine into the chamber through 6 mm Pyrex filters to simulate sunlight, achieving an intensity comparable to solar noon at mid-latitude in June and leading to a NO_2 photolysis frequency of $J_{NO2(CESAM)} = 7.3\times10^{-3}$ s^{-1}. Gas-phase HOOH was added continuously to the chamber after the given start time by flushing inlet oxygen through a bubbler containing concentrated aqueous HOOH solution. Water vapor is added via pulses of expansion-cooled steam from a stainless-steel boiler containing ultrapure water, after the first five batches of steam are vented to minimize any gas-phase contaminants. Depending on the specific experimental design, once the chamber is near water saturation, cloud events can be triggered by controlled pumping that removes 10% of the pressure in the chamber over a 10-min period. This pressure drop pushes the chamber at a controlled rate into supersaturation, forming a cloud whose evolving size distribution is characterized by a droplet spectrometer (PALAS welas, 0.5 to 15 μm). Conditions for each chamber experiment conducted in CESAM for this work are summarized in Table 1.

Table 1. Summary of Conditions of Guaiacol Photolysis and Photooxidation Chamber Experiments

Experiment	Seeds	RH_{max}(%)	[Guai] (ppb)[a]	HOOH	Lights	Comments
0	Na_2SO_4	>100	**0**	Yes	Yes	no guaiacol
1	**None**	>100	15 ±5	No	Yes	no seeds or HOOH
2	Na_2SO_4	**50**	8	No	Yes	solid seeds, no HOOH
3	Na_2SO_4	>100	38	Yes	Yes	standard
4	Na_2SO_4	>100	36	No	Yes	no HOOH
5	Na_2SO_4	**50**	43	Yes	Yes	solid seeds
6	$Na_2SO_4 + FeSO_4$	>100	27	No	Yes	with Fe^{3+}
7	$Na_2SO_4 + FeSO_4$	>100	27	Yes[b]	No	dark Fenton
8	$Na_2SO_4 + FeSO_4$	>100	25	Yes	Yes	photo-Fenton

Notes: **a**: equilibrium concentrations in humid chamber, quantified by PTR-MS after calibration by long-path FTIR. **b**: gas phase HOOH concentration measured by long-path FTIR was 1.9 ppm after 67 min of dark addition to dry chamber. All other experiments with HOOH involved addition to a humidified chamber; under these conditions HOOH could not be quantified by FTIR.

Gases in the chamber were quantified by NO_2 cavity (Teledyne T500U), NO_x chemiluminescence (Horiba APNA-370), SO_2 fluorescence (Horiba APSA-370), and ozone absorption monitors (Horiba APOA-370); CO / CO_2 infrared cavity sensors (ap2e ProCeas); PTR-MS (KORE II); and long-path in situ Fourier transform infrared (FTIR) instruments (Bruker Tensor 37, 184 m pathlength). Pseudo-first-order loss rate constants of butanol-*d9* measured at *m/z* = 66 by PTR-MS were divided by the known 2nd-order rate constant for the butanol-*d9* + OH radical reaction (k = 3.4 ±0.3) × 10^{-12} cm^3 $molec^{-1}$ s^{-1} at 295K)[21] to calculate average OH radical concentrations for each measurement period where butanol losses were observable. Each

measurement period was over an hour long, on average. Humidity was monitored by RH probes (Vaisala HMP234). Dried aerosol size distributions were measured by scanning mobility particle sizing (SMPS, TSI 3080 / 3772), while dried aerosol absorption was measured by a 7-wavelength dual-spot aethalometer (Magee AE33). Both instruments sampled aerosol through a Nafion drying tube. Aerosol chemistry was probed by a time-of-flight aerosol chemical speciation monitor (TOF ACSM) (Aerodyne, 6-min averaging), where the reading for organics (Org) was used to quantify SOA. Water-soluble aerosol components were sampled by a particle-into-liquid sampler (PILS, Brechtel Manufacturing Inc.); the absorbance of dissolved aerosol components in the PILS outflow was continuously monitored by a dual-beam waveguide UV-vis spectrometer (1 or 2 m pathlength, 200 – 800 nm, OceanOptics). To quantify BrC, PILS-waveguide absorption measured at 365 nm was converted to mass absorption coefficients (MAC) in $m^2\ g^{-1}$ using the equation

$$MAC = \frac{Abs_e}{bC\left(\frac{V_{sampled}}{V_{output}}\right)}$$

where Abs_e is the measured ln-based absorption at a given wavelength, b is the optical path length in m of the waveguide used, C is the organic aerosol (OA) concentration measured by ACSM in $g\ m^{-3}$, $V_{sampled}$ is the flow rate of PILS sampling from the chamber (7500 mL min^{-1}), and V_{output} is the PILS liquid outflow rate (0.33 to 0.50 mL min^{-1}, measured 1-2× daily). Atmospheric OH exposure times to reach maxima in SOA and BrC were calculated by multiplying the experimental times to each maxima (in h) by the calculated OH level and dividing by an atmospheric OH concentration of 1×10^6 molec/cm^3.

Results and Discussion

Experiments with sodium sulfate seeds. Table 2 summarizes key parameters obtained from the experiments conducted in this study. Long-path FTIR measurements during Experiment 7 indicated that HOOH concentrations reached 1.9 ppm after ~1 h of addition to the dark, dry chamber. HOOH could not be quantified by FTIR in other experiments due to water vapor interference. Experiments 0-2 and 4 were control experiments missing one or more of the reactants expected to be necessary for the aqueous-phase photooxidation of guaiacol: these experiments were performed without guaiacol, without seed aerosol and an OH radical source, without an aqueous phase and an OH source, and without an OH source, respectively. In Experiment 0 (Figure S1), conducted in the freshly-cleaned chamber before it had ever been exposed to guaiacol, ACSM organic signals – which we use to quantify SOA formation – increased by 2 $\mu g/m^3$ once RH exceeded 50%, and again by 2.8 $\mu g/m^3$ when chamber lights were turned on, indicating the presence some background contamination capable of aqueous SOA production. This SOA formation, totaling just under 5 $\mu g/m^3$, was defined as the background level for these experiments in the illuminated CESAM chamber. See section "SOA background level determination" and Table S1 in the online supplemental information (SI) document for additional details.

In Experiment 1 (Figure S2), conducted with gas-phase guaiacol but without seed particles or oxidant, new particles nucleated 12 min after chamber lights were turned on, as seen by the sudden increase of 8×10^4 cm^{-3} in SMPS counts. Both SMPS mass and ACSM organic signals increased by around 4 $\mu g/m^3$ during illumination in Experiment 1, comparable to the level of SOA formed without guaiacol in Experiment 0, suggesting the same background OH and/or SOA source, rather than guaiacol photolysis, was responsible. Guaiacol can be directly photolyzed by sub-actinic radiation (wavelengths in the 270 - 300 nm range). While the three solar simulator 6500 W Xe arc lamps filtered with 6 mm pyrex filters generate a small amount of light below 300 nm,[20] the

above comparison to the experiment without guaiacol suggests that direct photolysis of gas-phase guaiacol is not the major SOA source in this experiment. The maximum absorbance measured by PILS / waveguide UV-vis absorption spectroscopy at 365 nm was 0.022, near the absorption detection limit in Experiments 0-2 (performed with a 1 m waveguide) of 0.025. Other experiments were performed with a 2 m waveguide and thus have absorption detection limits of 0.0125.

Table 2. Summary of Guaiacol Photolysis and Photooxidation Chamber Experiments

Expt.	Fig.	Comments	SOA_{max} ($\mu g/m^3$)	$Abs_{max,}$ 365 nm	MAC_{365} ($m^2\ g^{-1}$)[a]	[OH][b] /10^6 molec cm^{-3}	Integrated [OH] to max MAC /10^6 molec cm^{-3} h	$OS_{C\ max}$[c]
0	S1	no guaiacol	< 5[d]	< 0.025[e]	n/a	--	n/a	1.38
1	S2	**no seeds or HOOH**	< 5[d]	< 0.025[e]	n/a	4.3	n/a	0.95
2	S3	solid seeds, no HOOH	< 5[d]	< 0.025[e]	n/a	9.6	n/a	1.25
3	1, S4	standard	21	0.12	0.29	14	5.8	1.62
4	2, S5	no HOOH	27	0.21	0.27	2.6	6.3	1.60
5	4, S6	solid seeds	11.5	0.18	1.14	9.8	6.1	1.60
6	S7	with Fe^{3+}	14	0.20	0.87	5.3	9.4	1.80
7	S8	dark Fenton	4.1[f]	0.035	0.94	9.9	1.0	2.02
8	5, S9	photo-Fenton	7.7	0.025	0.24	11	3.2	2.28

Notes: **a**: at time of maximum aerosol absorption. **b**: measured via 1st-order losses of butanol-*d9* during chamber illumination. **c**: maximum oxidation state of carbon calculated from TOF-ACSM data. **d**: chamber background SOA production level with solar simulations lights on, see SI for details. **e**: measured using a waveguide with a 1 m pathlength. All other experiments used a 2m waveguide and so have lower detection limits for absorption. **f**: Value is over 10× larger than dark chamber background SOA level, see SI for details.

In Experiment 2 (Figure S3), conducted without oxidant at 50% RH (too low to deliquesce the Na_2SO_4 seed particles), SOA and BrC formation levels after exposure to simulated sunlight were again at or below chamber background levels measured during Experiments 0 and 1. In this experiment the chamber was humidified before guaiacol addition to determine if more wall-bound guaiacol from Experiment 1 (see SI for further discussion of guaiacol-wall interactions) would be released back into the gas phase. Approximately 1 ppb of guaiacol was detected in the chamber immediately after water vapor addition, declining within 10 min to an equilibrium concentration of 0.2 ppb. This pattern of a burst of gas-phase guaiacol followed by a lower, steady-state concentration upon chamber humidification was observed in many experiments. The injection of additional gas-phase guaiacol into the chamber increased guaiacol PTR-MS signals to a new steady-state value corresponding to 8 ppb. As in Experiment 1, this value was stable until the solar simulator lights were turned on, at which point guaiacol concentrations decreased with a 30-min half-life. Since SOA and BrC production remained at background levels, we again conclude that direct photolysis of gas-phase guaiacol is occurring, but is not a significant source of SOA or BrC in these experiments without oxidants or deliquesced aerosol particles present.

Experiment 3 (Figures 1 and S4) was conducted by adding all the expected components for aqueous BrC formation: deliquesced seed particles, a gas-phase phenolic species (guaiacol) and a source of OH radicals (HOOH + solar simulator lights). After the lights were turned on and OH radicals were generated, SOA and BrC formation were observed, reaching maximum values of 21 $\mu g/m^3$ (org, panel d in Figure 1) and 0.29 $m^2\ g^{-1}$ MAC_{365} (converted from maximum 365-nm absorbance, panel c in Figure 1) within 23 min. After the maximum absorption was reached, aging by further OH radical photooxidation reduced absorption by 22% over the next 35 minutes. PTR-MS-measured pseudo-first-order loss rate constants for butanol-*d9* ($k' = 4.9 \times 10^{-5}\ s^{-1} = k[OH]$,

where k = (3.4 ±0.3) $\times 10^{-12}$ cm^3 molec^{-1} s^{-1} at 295K)[21] were used to calculate average OH radical concentrations of 14 $\times 10^6$ molec cm^{-3}, or a factor of 14 higher than average ambient levels. Thus, we estimate that in the atmosphere it would take 5.5 h of photooxidation to reach peak levels of aqSOA and BrC, if other conditions were equal.

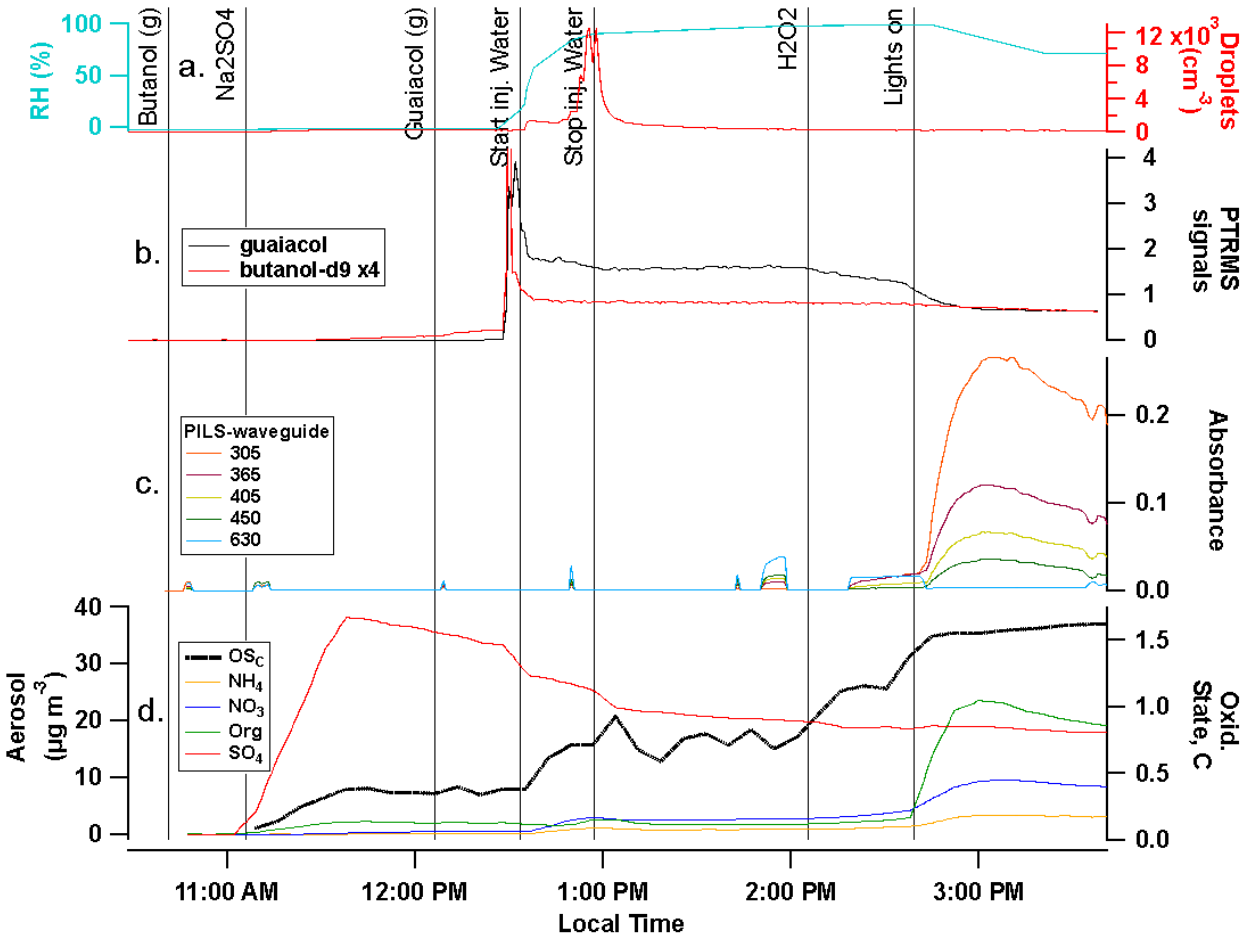

Figure 1: Experiment 3. Na_2SO_4 seeds, guaiacol, cloud event, and HOOH + lights. Panel **a**: RH (blue line) and droplet counts (red, right axis). **b**: PTR-MS signals for guaiacol (black line) and butanol-*d9* (red, multiplied by a factor of 4). **c**: absorbance measured in water-soluble aerosol particles by PILS / waveguide UV-vis, with absorbance below detection limit shown as flat baseline. **d**: average oxidation state of carbon (black line) and ACSM aerosol loadings after

dilution corrections, for sulfate (red), organic (green), nitrate (blue), and ammonium-assigned signals (orange).

Experiment 4 (Figures 2 and S5) was similar to Experiment 3 but conducted without adding HOOH as the OH radical source. As in Experiment 3, no chemistry was observed before the lights were turned on. After the lights were turned on, gas-phase guaiacol signals declined slowly (with a half-life of >150 min) and slow SOA and BrC formation were observed. SOA and BrC formation reached similar levels as when an OH source was present, but 2.4 hours of reaction time were required to reach the maximum, instead of 25 min. Thus, SOA and BrC formation was ~6× slower without an OH source present. However, the similarity in the O/C ratios and in the maximum MAC spectra (Figure 3) suggests that Experiments 3 and 4 reached similar chemical endpoints. This is consistent with guaiacol + OH chemistry happening in both experiments, but with a smaller quantity of radical species present in Experiment 4. Indeed, PTR-MS butanol-*d9* signals indicate that OH levels were 5.3× lower in Experiment 4, and the time to maximum SOA and BrC levels was longer by almost the same factor (5.8×). Photosensitization could generate triplet carbon ^3C radicals, which can react with dissolved oxygen to form these small amounts of OH and HO_2 radicals.[21] Since dissolved guaiacol has little absorption of light at wavelengths > 300 nm, it is a poor photosensitizer in bulk aqueous solution. However, a small amount of light below 300 nm is present in the CESAM chamber.[20] Furthermore, when guaiacol is adsorbed at ice surfaces its absorption spectrum is red-shifted,[22, 23] and its quantum yield for photodegradation increases by more than an order of magnitude.[23] Since molecular dynamics simulations indicate that guaiacol is surface active in water droplets,[24] it seems likely that similar effects at air-water interfaces might rationalize photosensitization by guaiacol in suspended aqueous aerosol.

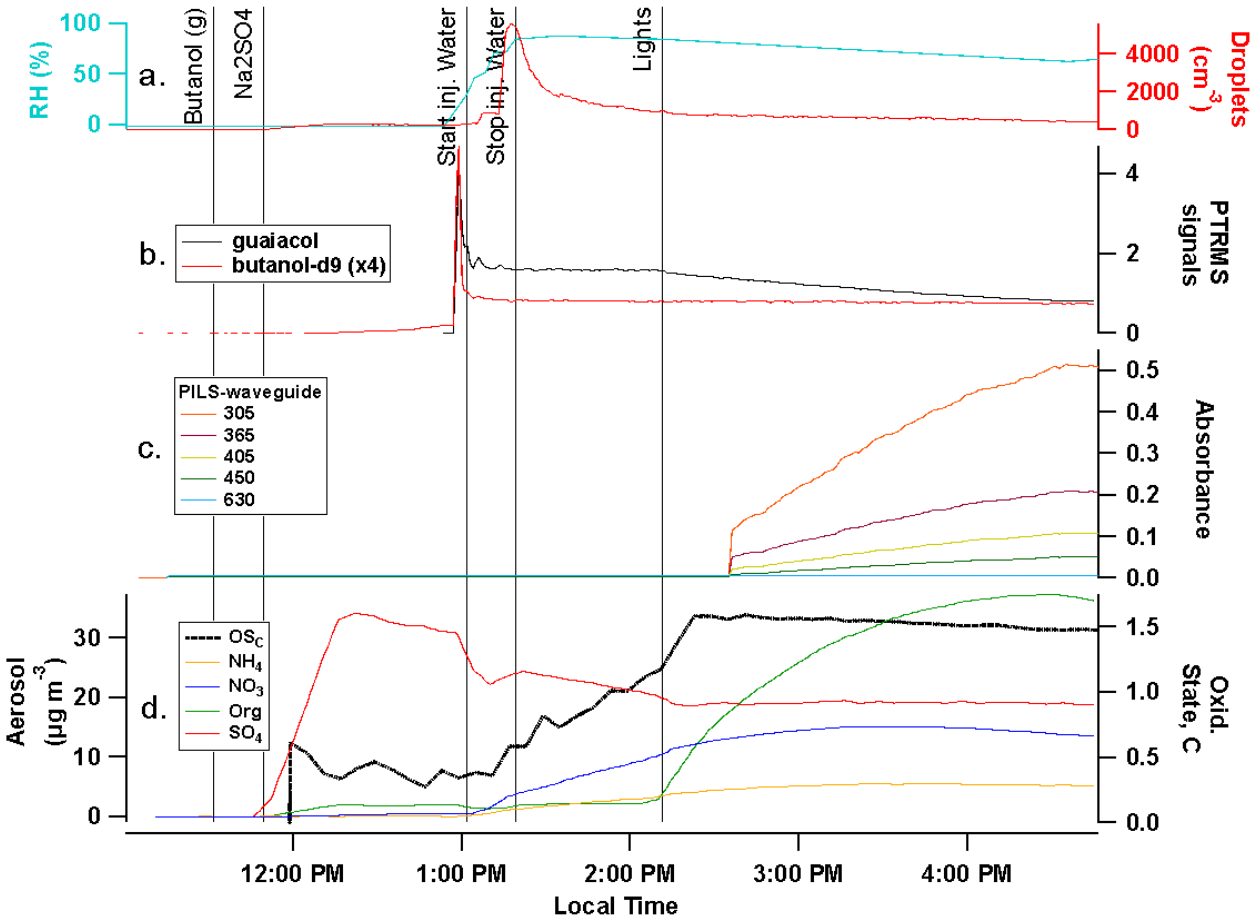

Figure 2: experiment 4 with Na_2SO_4 seed particles, gas-phase guaiacol, a cloud event, and simulated sunlight, but no HOOH. Panel **a**: RH (blue line) and droplet counts (red, right axis). **b**: PTR-MS signals for guaiacol (black line) and butanol-*d9* (red, multiplied by a factor of 4). **c**: absorbance measured in water-soluble aerosol particles by PILS / waveguide UV-vis, with absorbance below detection limit shown as flat baseline. **d**: average oxidation state of carbon (black line) and ACSM aerosol loadings after dilution corrections, for sulfate (red), organic (green), nitrate (blue), and ammonium-assigned signals (orange).

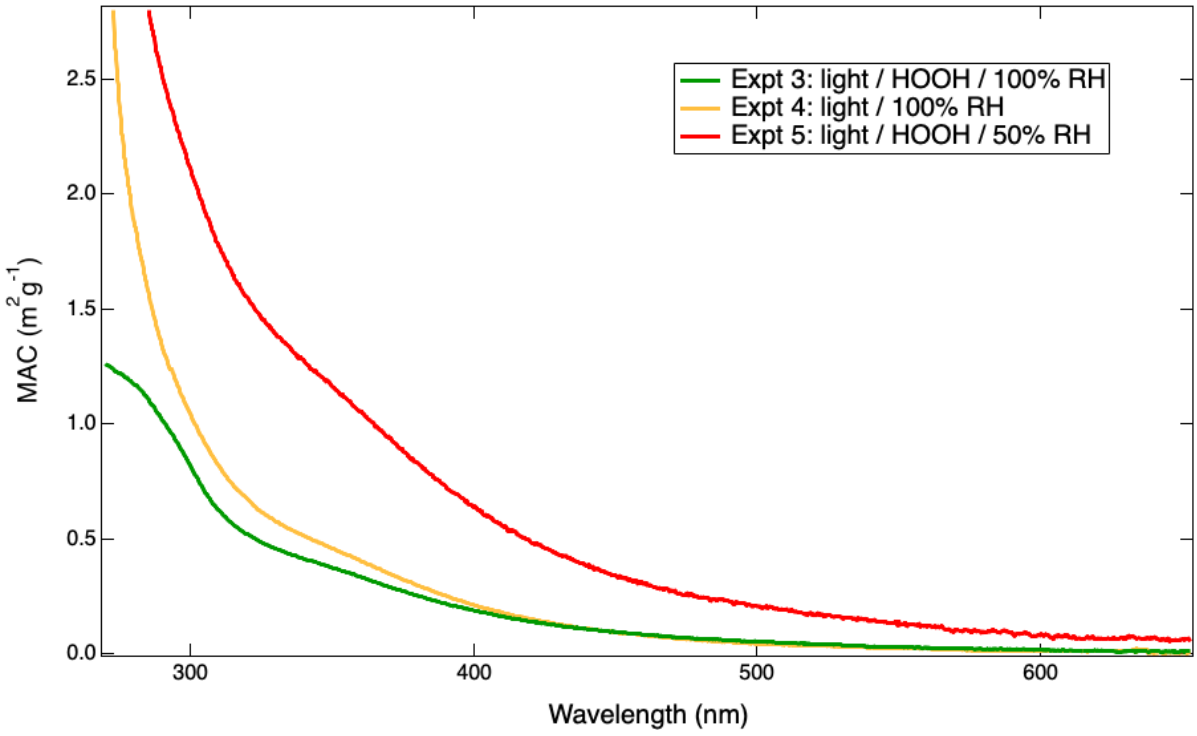

Figure 3: Maximum-magnitude MAC spectra recorded in guaiacol photooxidation experiments #3 (light/HOOH/100% RH), #4 (light/100% RH, no HOOH), and #5 (light/HOOH/50% RH).

In Experiment 5 (Figures 4 and S6), dry Na_2SO_4 aerosol was mixed with gas-phase guaiacol and HOOH at 50% RH. At this RH level, Na_2SO_4 aerosol particles do not deliquesce, and so no aqueous phase should be present. After solar simulator lights were turned on to generate OH radicals from HOOH, gas-phase guaiacol signals declined with a 20 min half-life and SOA formation was immediately detected by TOF ACSM. Approximately 10 minutes later, BrC formation was also detected by the PILS / waveguide and the aethalometer, reaching a maximum after another 25 min. In Experiment 2, performed at the same RH level but without HOOH present, SOA and BrC formation were minimal (at chamber background levels). We reason that when the OH photooxidation of guaiacol generated an SOA phase in Experiment 5, this SOA was hygroscopic enough to allow the aerosol particles to take up a little water at 50% RH, something

which pure Na_2SO_4 aerosol does not do.[25] Once this occurred over the first 10 min of photooxidation, condensed-phase photooxidation of guaiacol was able to begin in this "wet OA" phase, generating BrC with a peak MAC_{365} value almost 4 times larger than in Experiments 3 or 4 conducted with deliquesced seed particles near 100% RH (Figure 3). Thus, more strongly-absorbing BrC can be formed from condensed-phase guaiacol photooxidation in guaiacol SOA at 50% RH than in deliquesced Na_2SO_4 / SOA aerosol near 100% RH, likely due to more efficient BrC oligomer formation in a condensed phase with higher concentrations of organic species and less water.

In Experiments 3-5, the time to maximum SOA concentrations, expressed in integrated gas-phase OH concentrations, was consistently t_{OH} = (5.3 ±0.6) ×10^6 molec cm^{-3} h, or an atmospheric oxidation time of 5.3 h. The maximum BrC absorption was reached at nearly the same integrated OH time, t_{OH} = (6.0 ±0.3) ×10^6 molec cm^{-3} h, or an atmospheric oxidation time of 6.0 h, in Experiments 3-5. This good agreement is remarkable because BrC production is driven by reactions with aqueous-phase OH radicals, which are produced mainly *in situ* by aqueous-phase HOOH photolysis, rather than by uptake from the gas phase, especially in large or viscous aerosol particles. However, for surface-active chemical species like guaiacol that are predicted to be absorbed at or near the air-water interface,[24] good agreement between integrated gas-phase OH exposure and BrC level maxima would be expected.

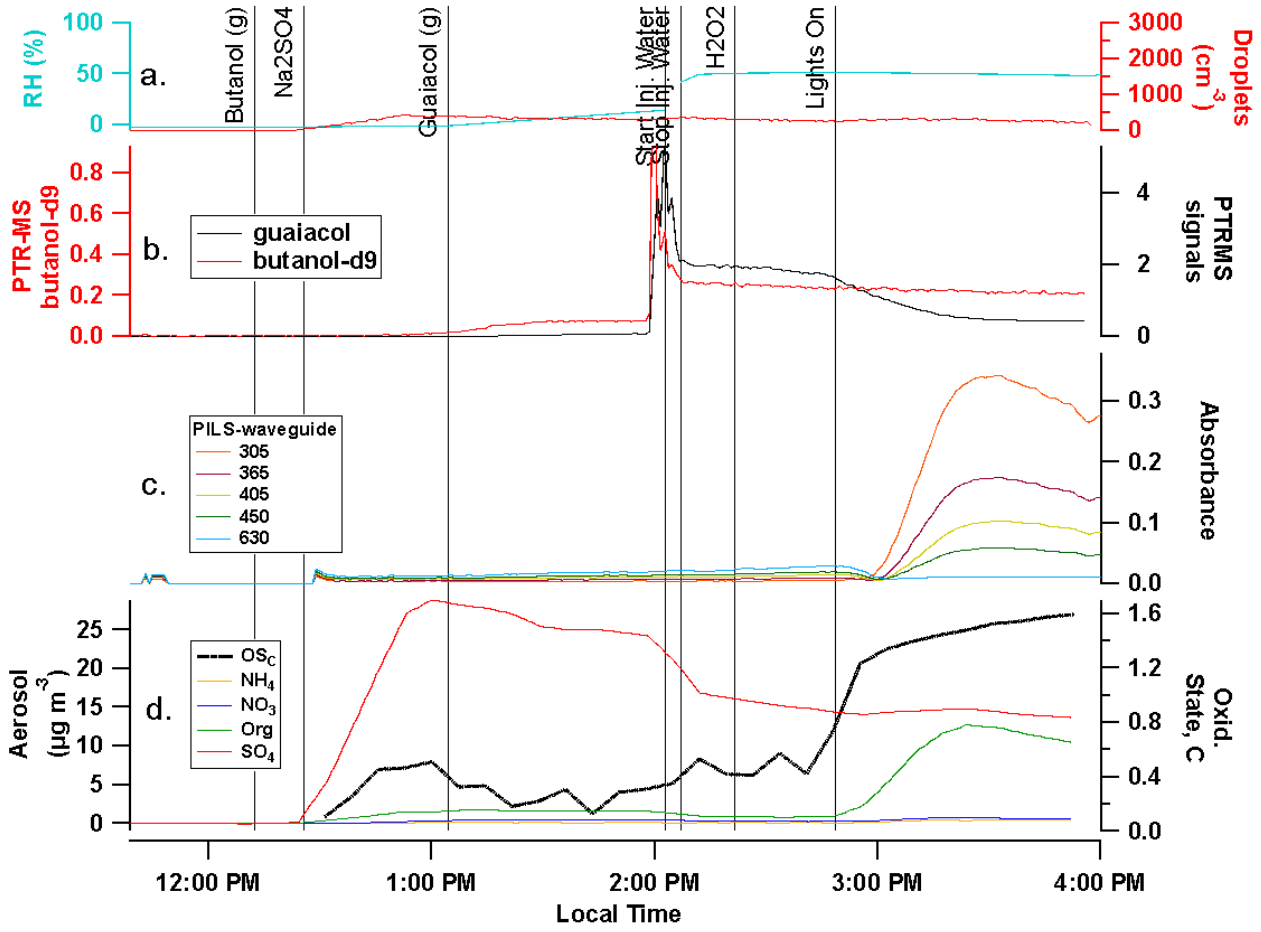

Figure 4: Experiment 5, performed at 50% RH with undeliquesced Na_2SO_4 seeds, guaiacol, and HOOH + lights. Panel **a**: RH (blue line) and droplet counts (red, right axis). **b**: PTR-MS signals for guaiacol (black line) and butanol-*d9* (red, left axis). **c**: absorbance measured in water-soluble aerosol particles by PILS / waveguide UV-vis, with absorbance below detection limit shown as flat baseline. **d**: average oxidation state of carbon (black line) and ACSM aerosol loadings after dilution corrections, for sulfate (red), organic (green), nitrate (blue), and ammonium-assigned signals (orange).

In these three experiments (3, 4, and 5) the oxidation state of SOA carbon measured by ACSM also reached a highly consistent maximum of 1.61 ±0.02 (Figures 1, 2, and 4), significantly

exceeding OS_C values observed in prior bulk liquid or dry chamber guaiacol photooxidation studies (+0.51). [1, 7, 8] The OS_C of freshly-formed SOA (measured within the first 12 min) was +1.57 ±0.02 in Experiments 3 and 4 when SOA was formed near 100% RH, and +1.34 when formed at 50% RH in Experiment 5. The effect of aging on OS_C depended on whether HOOH was added. In Experiments 3 and 5 where HOOH was added, OS_C slowly but continuously increased, likely due to OH radical reactions in the dilute aqueous or more concentrated "wet OA" phase. In Experiment 4, without HOOH added (Figures 2 and S5), OS_C slowly declined after the SOA phase was established, suggesting that SOA growth is dominated in this case by the partitioning of more volatile, less oxidized organic species into the growing SOA phase,[26] rather than aerosol-phase oxidation reactions. The extremely high OS_C values measured in these experiments also suggests that small carboxylate species such as oxalates and formates are major contributors to SOA mass, consistent with an earlier study where organic acid functionalities were found to make up 77% of the oxygen in guaiacol + OH SOA formed under dry conditions.[27]

To summarize, BrC production during guaiacol photooxidation can occur either in deliquesced inorganic aerosol or in guaiacol SOA at 50% RH, with rates of SOA and BrC production directly proportional to gas-phase oxidant concentrations. In all cases, the SOA formed in suspended aqueous aerosol particles is very highly oxidized compared to previous studies of bulk aqueous or dry guaiacol photooxidation, even after the equivalent of only a few hours of atmospheric OH exposure.

Experiments with seeds containing soluble iron. Experiments 6-8 were conducted with seeds generated from 10 mM Na_2SO_4 / 0.31 mM $FeSO_4$. In Experiment 6 (Figure S7), other conditions were similar to Experiment 4: both experiments had deliquesced seed particles and solar simulator

lights were on at the end of the experiment, but no HOOH present. Experiment 6 had guaiacol concentrations that were 25% lower, in addition to aerosol-phase Fe^{2+} ions. The two experiments produced broadly similar results: SOA and BrC production was slow, occurred only after solar simulator lights were turned on, and took over an hour to reach maxima, with SOA peaking before BrC by at least 30 min. While only half as much SOA was produced with photolysis in Experiment 6, peak absorption measured at 365 nm was almost identical to Experiment 4, resulting in a significantly larger peak MAC_{365} value in the presence of soluble Fe^{2+} ions. Furthermore, peak SOA and BrC levels were reached in Experiment 6 at integrated OH exposures of 7.7×10^6 and 9.4×10^6 molec cm^{-3} h (or 7.7 and 9.4 h atmospheric photooxidation time, respectively), or ~50% higher OH exposures than in Experiments 3-5 without soluble iron. Thus, BrC formed from guaiacol photooxidation in the presence of soluble iron is both more abundant and more resistant to photobleaching than in the absence of iron.

SOA in Experiment 6 was also more highly oxidized: the OS_C of freshly generated SOA was 1.80 (instead of 1.59), and then slowly declined, as in Experiment 4. These observations suggest that, as in Experiment 4, small amounts of oxidants are generated via photosensitization when the lights are turned on, where surface-adsorbed guaiacol is the likely photosensitizing species reacting with dissolved oxygen. These oxidants react with additional guaiacol to generate SOA and BrC at a slow rate, and also convert some Fe^{2+} to Fe^{3+}. Redox reactions between Fe^{3+} and organic SOA species could then further oxidize the SOA, raising the OS_C beyond what was observed in the absence of soluble iron, while favoring oligomerization processes at the expense of fragmentation and photobleaching.

In Experiment 7 (Figure S8), gas-phase HOOH was added to the dark chamber after Na_2SO_4 / $FeSO_4$ seeds and gas-phase guaiacol. In the (dark) Fenton reaction, HOOH dissolved in an acidic

aqueous solution oxidizes Fe^{2+} ions to Fe^{3+} while generating a hydroxyl radical, which will then oxidize other organic species. Fe^{3+} + phenolic compound redox reactions can return iron to the +2 oxidation state to repeat the entire process until HOOH is depleted. When all the chemical ingredients were present in the chamber for the Fenton reaction to occur (*i.e.* HOOH(g), guaiacol(g), and aerosol-phase Fe^{2+}), no reaction occurred until the RH was increased past ~60%, a level well below the deliquescence relative humidity (DRH) of 93% for Na_2SO_4. DRH for $FeSO_4$ is greater than 93%,[28] but at 65% RH mono- and tetra-hydrate forms of iron sulfate transition to a heptahydrate,[29] which may create an amorphous surface that adsorbs enough water[30] for aqueous Fenton chemistry to begin. Once the increasing RH reached 65% in Experiment 7, small amounts of SOA (4.1 μg/m^3, org, panel c) and BrC formation were observed as RH continued to increase, but BrC absorption was above the waveguide detection limit for less than 20 minutes, and little absorption was observed by the aethalometer. Maxima in SOA and BrC levels were observed at integrated OH levels of 3.6×10^6 molec cm^{-3} h and 1.0×10^6 molec cm^{-3} h, significantly lower than in other experiments. There are several possible explanations for the low build-up and quick loss of BrC absorption, which we will explore here. First, excess HOOH or Fe^{3+} could efficiently oxidize and destroy BrC or BrC-precursor species formed by the guaiacol + OH reaction. Second, the guaiacol + Fe^{3+} reaction could fail to produce BrC in aqueous aerosol particles, even though this process is efficient in bulk acidic aqueous solution.[15, 16, 31] Third, HOOH or OH radicals could destroy BrC produced by the guaiacol + Fe^{3+} reaction.

While excess HOOH has been observed to destroy brown carbon compounds as they form in aqueous reactions between aldehydes and amines,[32] we note that guaiacol + OH BrC formed readily in the presence of HOOH in experiments 3 and 5, and was clearly enhanced in the presence of iron (suggesting at least some Fe^{2+} - Fe^{3+} cycling) in Experiment 6, so the first possible

explanation is unlikely. Experiment 6 also demonstrated that guaiacol + Fe^{3+} reactions enhanced BrC formation in suspended aqueous aerosol particles, just like it did in earlier bulk aqueous experiments,[15, 16, 31] eliminating the second explanation. We conclude, therefore, that BrC produced by the guaiacol + Fe^{3+} reaction, including insoluble BrC polymers, appears to be rapidly oxidized by the high concentrations of OH radicals produced in the aqueous phase by the Fenton reaction.

While the gas-phase concentration of OH radicals inferred from PTR-MS butanol-*d9* loss rates in Experiment 7 is nearly identical to that measured in Experiment 5, we reason that the extra OH radicals generated in the aqueous aerosol phase by Fenton chemistry in Experiment 7 will overwhelmingly react in that phase, rather than escaping to the gas phase. In other words, while gas- and aqueous-phase OH radical production from the same precursor (HOOH) in experiments 3-6 could be expected to be correlated, the addition of Fenton chemistry eliminates that correlation by raising aqueous OH radical production without significantly influencing measured gas-phase OH concentrations. If BrC produced from guaiacol + OH and guaiacol + Fe^{3+} reactions are similar in their resistance to photobleaching, the fact that BrC peaks 6× earlier in Experiment 7 in terms of integrated gas-phase OH concentrations suggests that average OH concentrations in the aqueous phase were approximately 6× higher in Experiment 7. In other words, Fenton chemistry appears to have raised the aqueous OH concentrations by a factor of ~6 compared to that produced by HOOH photolysis.

Notably, in Experiment 7 ACSM-measured OS_C reached a peak value of 2.02, suggesting significant oxidation of SOA material by Fe^{3+} redox reactions and by OH radicals produced by Fenton chemistry. Such a high OS_C indicates that carboxylic acids, especially oxalic acid (with $OS_C = 3.0$), are the dominant organic species present, since carboxylate is the only functional group

producing OS_C values in this range. Additionally, it is evident that the aqueous SOA was acidic enough – from organic acid production – to allow Fenton chemistry to proceed, even though the seed particles were not initially acidified.

In Experiment 8 (Figures 5 and S9), lights were turned on near the end of the experiment to allow photo-Fenton chemistry to occur. Under these conditions, after Fe^{2+} is oxidized by HOOH in acidic solution to produce Fe^{3+} and a hydroxyl radical, sunlight contributes to the reduction of Fe^{3+} back to Fe^{2+} and accelerates the cycling between Fe^{2+} and Fe^{3+} and therefore the production of OH radicals.[18] Once the lights were turned on in Experiment 8, BrC reached maximum absorbance and SOA reached a maximum of 7.7 $\mu g/m^3$ within 15 minutes, the shortest time to an SOA maximum in any experiment. SOA and BrC maxima corresponded with integrated gas-phase OH exposure levels of 2.7 $\times 10^6$ molec cm^{-3} h and 3.2 $\times 10^6$ molec cm^{-3} h, or about half the OH exposure required in Experiments 3-5. As in Experiment 7, aqueous phase OH production by photo-Fenton chemistry was likely decoupled from gas-phase OH levels generated by HOOH photolysis, so the halved time to maximum SOA and BrC levels therefore implies an enhancement of aqueous-phase OH concentrations by a factor of ~2× relative to Experiments 3-5. OS_C reached 2.28, the highest of any experiment, within 30 minutes. While the quantities of SOA and BrC absorption in Experiment 8 were much smaller than in Experiment 3 (without soluble iron), the MAC was similar in the two experiments. The short timescales to maxima in SOA and BrC signals and the extremely high OS_C measured by ACSM suggest that the photo-Fenton reaction generated very high oxidant levels in the aqueous phase, as expected,[18] and that these high oxidant levels quickly generated, and then destroyed, SOA and BrC aerosol species.

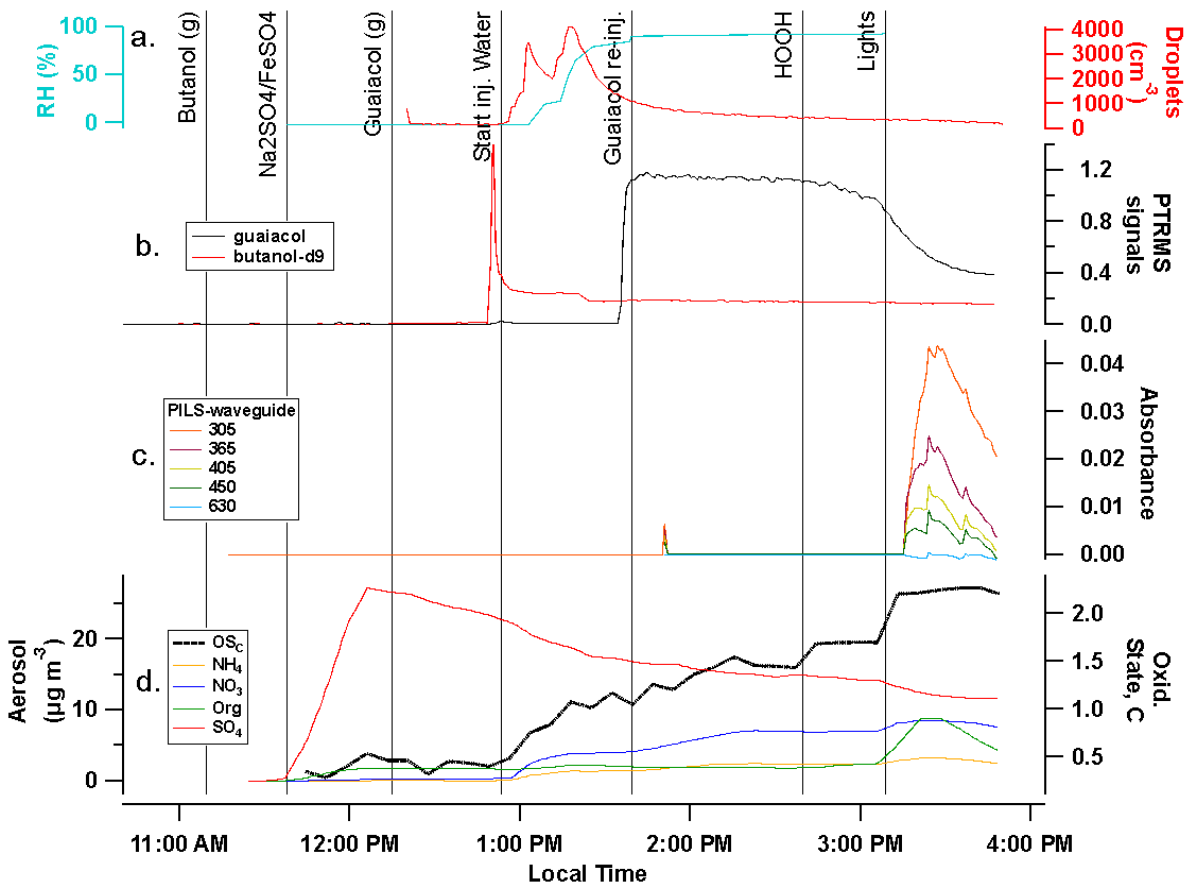

Figure 5: Experiment 8. Photo-Fenton chemistry aerosol experiment with Na_2SO_4 / $FeSO_4$ seeds, guaiacol, high RH, and HOOH + lights. Panel **a**: RH% (blue line) and droplet counts (red, right axis). **b**: PTR-MS signals for guaiacol (black line) and butanol-*d9* (red). **c**: absorbance measured in water-soluble aerosol particles by PILS / waveguide UV-vis, with absorbance below detection limit shown as flat baseline. **d**: average oxidation state of carbon (black line) and ACSM aerosol loadings after dilution corrections, for sulfate (red), organic (green), nitrate (blue), and ammonium-assigned signals (orange).

The insoluble BrC production that occurs in the dark when acidic Fe^{3+} and guaiacol are mixed in bulk aqueous solutions[15, 16, 31] should be detected by the aethalometer in these experiments. However, in Experiment 8 when guaiacol was injected into the dark chamber containing

deliquesced Na_2SO_4 / $FeSO_4$ seeds at 13:35 and then HOOH was added at 14:39 to convert Fe^{2+} to Fe^{3+}, no increase in absorption was recorded by the aethalometer, likely due to a lack of acidity, since photooxidation had not yet begun, and seed particles were not acidified. When the solar simulator lights were turned on at 15:08 and acidic SOA was formed, at this point all necessary reactants for insoluble BrC polymer production would seem to be present in Experiment 8, and yet aethalometer signals did not increase at any wavelength, and soon declined and reached negative values. Since the aethalometer integrates absorption of aerosol particles as they build up on a filter, the measurement of negative values indicates that BrC species already on the filter were getting destroyed by oxidants sampled along with chamber aerosol. Again, while our seed aerosol particles were not acidified, the very high OS_C level indicates that carboxylic acids were the major SOA components, and that the acidic photo-Fenton reaction was generating high levels of oxidants. Insoluble BrC polymers, if formed as anticipated in these experiments by dark reactions between guaiacol and soluble iron in an acidified aqueous phase, must have been rapidly photobleached or destroyed by high levels of oxidants and therefore could not be detected.

To summarize, the addition of soluble iron to seed aerosol particles enhanced production of SOA and BrC during photooxidation in the absence of HOOH, likely due to the production of insoluble guaiacol oligomers. When HOOH was also added, however, the production of aerosol-phase oxidants via Fenton chemistry was high enough to heavily oxidize the SOA and quickly destroy BrC, more than offsetting the increases caused by adding iron.

Atmospheric Significance

Our results suggest that the oxidation chemistry of phenolic species like guaiacol in organic aerosol and aqueous (deliquesced) aerosol phases are not categorically different. Specifically, BrC

formation by guaiacol + OH was found to require the presence of either deliquesced inorganic aerosol or the presence of SOA at 50% RH. Most aerosol particles in the troposphere contain significant amounts of SOA material,[33] and the RH is above 50% in much of the lower troposphere, with the main exception being over desert areas during the day. Thus, we anticipate that "aqueous" BrC formation chemistry involving guaiacol and other phenolic species can likely occur in much of the troposphere, rather than only near or inside of clouds.

In non-iron-containing aerosol particles where HOOH photolysis is the most important source of OH radicals, we find that BrC generated by the guaiacol + OH reaction reaches a maximum at ~6 h of atmospheric OH exposure. This is roughly consistent with the photobrowning / photobleaching behavior observed in primary biomass burning aerosol[34] and some field-sampled smoke plumes, where photobrowning can be observed during the first 2-6 h of transport.[35] Since guaiacol + OH chemistry generates a significant percentage of SOA formation in smoke plumes,[4] this similarity is expected, and helps explain the observed evolution in optical properties of aerosol particles inside smoke plumes.

Smoke plumes often contain iron due to thermal convection of mineral dust during wildfires or to mixing with anthropogenic air masses,[36] and this iron can be solubilized during transport by acids or oxalate.[36-39] In the presence of soluble iron, additional BrC is generated by the guaiacol + Fe^{3+} redox reaction,[15, 16, 31] but this BrC (including insoluble polymers) is much more easily destroyed by OH photooxidation than is BrC produced by the aqueous-phase guaiacol + OH reaction. Fenton chemistry involving soluble iron and HOOH can quickly generate the OH radicals to accomplish this destruction of guaiacol + Fe^{3+} BrC. Thus, the contribution of iron to atmospheric BrC production by guaiacol is expected to depend very sensitively on the availability of HOOH. In the presence of adequate HOOH concentrations, aerosol-phase iron can be expected

to reduce guaiacol SOA and BrC through excessive oxidation, while at low HOOH, iron will increase guaiacol BrC formation.

Average SOA carbon oxidation states achieved in this study are significantly higher than those previously observed for dry photooxidation[1] or bulk liquid photooxidation of guaiacol,[7, 8] and also higher than observed for atmospheric particles, even after fractionation.[40] This indicates that, first, guaiacol photooxidation is a multiphase process enhanced at aerosol droplet surfaces, which cannot be satisfactorily simulated in bulk aqueous experiments. Second, our data suggests that guaiacol photooxidation in aerosol particles and cloud droplets can be an important source of very highly oxidized SOA material, especially oxalate. This contribution will be especially important in smoke plumes, where guaiacol is a significant gas-phase component.[4]

Supporting Information.

The following files are available free of charge. Description of how chamber SOA background levels were defined and quantified, summary of guaiacol-wall interactions, and summary graphs for Experiments 0-8. (PDF)

Corresponding Author

*David De Haan, Department of Chemistry and Biochemistry, University of San Diego, 5998 Alcala Park, San Diego CA 92110, USA. ddehaan@sandiego.edu

ACKNOWLEDGMENT

This work was funded by NSF grants AGS-1826593 and AGS-2218491. CNRS-INSU is gratefully acknowledged for supporting CESAM as an open facility through the National Instrument label. This project/work has received funding from the European Union's Horizon 2020 research and innovation programme through the EUROCHAMP-2020 Infrastructure Activity under grant agreement No 730997. AERIS/ACTRIS is acknowledged for supporting the Eurochamp data center.

DATA AVAILABILITY

Concentration-time profiles for the CESAM chamber experiments are freely accessible in .edf format through the chamber database at data.eurochamp.org maintained by AERIS for the benefit of ACTRIS ERIC. (Expt. 0: https://doi.org/10.25326/19PZ-7K35. Expt. 1: https://doi.org/10.25326/S4HH-AE54. Expt. 2: https://doi.org/10.25326/GC8M-4084. Expt. 3: https://doi.org/10.25326/F2K0-2113. Expt. 4: https://doi.org/10.25326/2PG4-BB05. Expt. 5: https://doi.org/10.25326/KV19-K863. Expt. 6: https://doi.org/10.25326/Z928-H697. Expt. 7: https://doi.org/10.25326/QYT0-8041. Expt. 8: https://doi.org/10.25326/GVD2-FS26).

ABBREVIATIONS

SOA, secondary organic aerosol; OA, organic aerosol; OS_C, oxidation state of carbon; BrC, brown carbon; CESAM, chamber for experimental multiphase atmospheric simulation; PILS, particle into liquid sampler; PTR-MS, proton transfer reaction mass spectrometer; RH, relative humidity; FTIR, Fourier transform infrared spectroscopy; SMPS, scanning mobility particle sizing; TOF ACSM, time-of-flight aerosol chemical speciation monitor; MAC, mass absorption coefficient; UV-vis, ultraviolet and visible.

REFERENCES

1. Yee, L. D.; Kautzman, K. E.; Loza, C. L.; Schilling, K. A.; Coggon, M. M.; Chhabra, P. S.; Chan, M. N.; Chan, A. W. H.; Hersey, S. P.; Crounse, J. D.; Wennberg, P. O.; Flagan, R. C.;

Seinfeld, J. H., Secondary organic aerosol formation from biomass burning intermediates: phenol and methoxyphenols. *Atmos. Chem. Phys.* **2013,** *13*, (16), 8019-8043. doi:10.5194/acp-13-8019-2013
2. Schauer, J. J.; Kleeman, M. J.; Cass, G. R.; Simoneit, B. R. T., Measurement of Emissions from Air Pollution Sources. 3. C1−C29 Organic Compounds from Fireplace Combustion of Wood. *Environ Sci Technol* **2001,** *35*, (9), 1716-1728. doi:10.1021/es001331e
3. Liu, C.; Liu, J.; Liu, Y.; Chen, T.; He, H., Secondary organic aerosol formation from the OH-initiated oxidation of guaiacol under different experimental conditions. *Atmos. Environ.* **2019,** *207*, 30-37. doi:https://doi.org/10.1016/j.atmosenv.2019.03.021
4. Akherati, A.; He, Y.; Coggon, M. M.; Koss, A. R.; Hodshire, A. L.; Sekimoto, K.; Warneke, C.; de Gouw, J.; Yee, L.; Seinfeld, J. H.; Onasch, T. B.; Herndon, S. C.; Knighton, W. B.; Cappa, C. D.; Kleeman, M. J.; Lim, C. Y.; Kroll, J. H.; Pierce, J. R.; Jathar, S. H., Oxygenated Aromatic Compounds are Important Precursors of Secondary Organic Aerosol in Biomass-Burning Emissions. *Environ Sci Technol* **2020,** *54*, (14), 8568-8579. doi:10.1021/acs.est.0c01345
5. Mabato, B. R. G.; Li, Y. J.; Huang, D. D.; Wang, Y.; Chan, C. K., Comparison of aqueous secondary organic aerosol (aqSOA) product distributions from guaiacol oxidation by non-phenolic and phenolic methoxybenzaldehydes as photosensitizers in the absence and presence of ammonium nitrate. *Atmos. Chem. Phys.* **2023,** *23*, (4), 2859-2875. doi:10.5194/acp-23-2859-2023
6. Smith, J. D.; Kinney, H.; Anastasio, C., Phenolic carbonyls undergo rapid aqueous photodegradation to form low-volatility, light-absorbing products. *Atmos. Environ.* **2016,** *126*, 36-44. doi:http://dx.doi.org/10.1016/j.atmosenv.2015.11.035
7. Sun, Y. L.; Zhang, Q.; Anastasio, C.; Sun, J., Insights into secondary organic aerosol formed via aqueous-phase reactions of phenolic compounds based on high resolution mass spectrometry. *Atmos. Chem. Phys.* **2010,** *10*, (10), 4809-4822. doi:10.5194/acp-10-4809-2010
8. Yu, L.; Smith, J.; Laskin, A.; Anastasio, C.; Laskin, J.; Zhang, Q., Chemical characterization of SOA formed from aqueous-phase reactions of phenols with the triplet excited state of carbonyl and hydroxyl radical. *Atmos. Chem. Phys.* **2014,** *14*, (24), 13801-13816. doi:10.5194/acp-14-13801-2014
9. Chang, J. L.; Thompson, J. E., Characterization of colored products formed during irradiation of solutions containing H_2O_2 and phenolic compounds. *Atmos. Environ.* **2010,** *44*, 541-551. doi:10.1016/j.atmosenv.2009.10.042
10. Li, Y. J.; Huang, D. D.; Cheung, H. Y.; Lee, A. K. Y.; Chan, C. K., Aqueous-phase photochemical oxidation and direct photolysis of vanillin - a model compound of methoxy phenols from biomass burning. *Atmos. Chem. Phys.* **2014,** *14*, (6), 2871-2885, doi:10.5194/acp-14-2871-2014
11. Romonosky, D. E.; Laskin, A.; Laskin, J.; Nizkorodov, S. A., High-Resolution Mass Spectrometry and Molecular Characterization of Aqueous Photochemistry Products of Common Types of Secondary Organic Aerosols. *J. Phys. Chem.* **2014,** *119*, (11), 2594-2606. doi:10.1021/jp509476r
12. Lauraguais, A.; Coeur-Tourneur, C.; Cassez, A.; Deboudt, K.; Fourmentin, M.; Choël, M., Atmospheric reactivity of hydroxyl radicals with guaiacol (2-methoxyphenol), a biomass burning emitted compound: Secondary organic aerosol formation and gas-phase oxidation products. *Atmos. Environ.* **2014,** *86*, 155-163. doi:https://doi.org/10.1016/j.atmosenv.2013.11.074

13. Ahmad, W.; Coeur, C.; Tomas, A.; Fagniez, T.; Brubach, J.-B.; Cuisset, A., Infrared spectroscopy of secondary organic aerosol precursors and investigation of the hygroscopicity of SOA formed from the OH reaction with guaiacol and syringol. *Applied Optics* **2017,** *56*, (11), E116-E122. doi:10.1364/AO.56.00E116
14. Kitanovski, Z.; Cusak, A.; Grgic, I.; Claeys, M., Chemical characterization of the main products formed through aqueous-phase photonitration of guaiacol. *Atmos. Meas. Tech.* **2014,** *7*, (8), 2457-2470, 14 pp. doi:10.5194/amt-7-2457-2014
15. Slikboer, S.; Grandy, L.; Blair, S. L.; Nizkorodov, S. A.; Smith, R. W.; Al-Abadleh, H. A., Formation of Light Absorbing Soluble Secondary Organics and Insoluble Polymeric Particles from the Dark Reaction of Catechol and Guaiacol with Fe(III). *Environ Sci Technol* **2015,** *49*, (13), 7793-7801. doi:10.1021/acs.est.5b01032
16. Lavi, A.; Lin, P.; Bhaduri, B.; Carmieli, R.; Laskin, A.; Rudich, Y., Characterization of Light-Absorbing Oligomers from Reactions of Phenolic Compounds and Fe(III). *ACS Earth and Space Chemistry* **2017,** *1*, (10), 637-646. doi:10.1021/acsearthspacechem.7b00099
17. Chin, H.; Hopstock, K. S.; Fleming, L. T.; Nizkorodov, S. A.; Al-Abadleh, H. A., Effect of aromatic ring substituents on the ability of catechol to produce brown carbon in iron(iii)-catalyzed reactions. *Environmental Science: Atmospheres* **2021,** *1*, (2), 64-78. doi:10.1039/D0EA00007H
18. Nguyen, T. B.; Coggon, M. M.; Flagan, R. C.; Seinfeld, J. H., Reactive Uptake and Photo-Fenton Oxidation of Glycolaldehyde in Aerosol Liquid Water. *Environ. Sci. Technol.* **2013,** *47*, (9), 4307-4316. doi:10.1021/es400538j
19. Kroflič, A.; Anders, J.; Drventić, I.; Mettke, P.; Böge, O.; Mutzel, A.; Kleffmann, J.; Herrmann, H., Guaiacol Nitration in a Simulated Atmospheric Aerosol with an Emphasis on Atmospheric Nitrophenol Formation Mechanisms. *ACS Earth and Space Chemistry* **2021,** *5*, (5), 1083-1093. doi:10.1021/acsearthspacechem.1c00014
20. Wang, J.; Doussin, J. F.; Perrier, S.; Perraudin, E.; Katrib, Y.; Pangui, E.; Picquet-Varrault, B., Design of a new multi-phase experimental simulation chamber for atmospheric photosmog, aerosol and cloud chemistry research. *Atmos. Meas. Tech.* **2011,** *4*, 2465-2494. doi:10.5194/amt-4-2465-2011
21. Anastasio, C.; Faust, B. C.; Rao, C. J., Aromatic Carbonyl Compounds as Aqueous-Phase Photochemical Sources of Hydrogen Peroxide in Acidic Sulfate Aerosols, Fogs, and Clouds. 1. Non-Phenolic Methoxybenzaldehydes and Methoxyacetophenones with Reductants (Phenols). *Environ Sci Technol* **1997,** *31*, (1), 218-232. doi:10.1021/es960359g
22. Bononi, F. C.; Chen, Z.; Rocca, D.; Andreussi, O.; Hullar, T.; Anastasio, C.; Donadio, D., Bathochromic Shift in the UV–Visible Absorption Spectra of Phenols at Ice Surfaces: Insights from First-Principles Calculations. *The Journal of Physical Chemistry A* **2020,** *124*, (44), 9288-9298. doi:10.1021/acs.jpca.0c07038
23. Hullar, T.; Bononi, F. C.; Chen, Z.; Magadia, D.; Palmer, O.; Tran, T.; Rocca, D.; Andreussi, O.; Donadio, D.; Anastasio, C., Photodecay of guaiacol is faster in ice, and even more rapid on ice, than in aqueous solution. *Environmental Science: Processes & Impacts* **2020,** *22*, (8), 1666-1677. doi:10.1039/D0EM00242A
24. Karlsson, B. C. G.; Friedman, R., Dilution of whisky – the molecular perspective. *Sci. Rep.* **2017,** *7*, (1), 6489. doi:10.1038/s41598-017-06423-5
25. Wijnhorst, R.; Demmenie, M.; Jambon-Puillet, E.; Ariese, F.; Bonn, D.; Shahidzadeh, N., Softness of hydrated salt crystals under deliquescence. *Nature Communications* **2023,** *14*, (1), 1090. doi:10.1038/s41467-023-36834-0

26. Pankow, J. F., An absorption model of the gas/aerosol partitioning involved in the formation of secondary organic aerosol. *Atmos. Environ.* **1994,** *28*, (2), 189-193.
27. Chhabra, P. S.; Ng, N. L.; Canagaratna, M. R.; Corrigan, A. L.; Russell, L. M.; Worsnop, D. R.; Flagan, R. C.; Seinfeld, J. H., Elemental composition and oxidation of chamber organic aerosol. *Atmos. Chem. Phys.* **2011,** *11*, (17), 8827-8845. doi:10.5194/acp-11-8827-2011
28. Jameson, L. A. An Investigation of the Deliquescence of Ferricopiapite and the Onset of Deliquescence of Epsomite Crystal Faces of Differing Miller Indices. M.Sc. thesis, Queen's University, Kingston, Ontario, Canada, 2011.
29. Mitchell, A. G., The preparation and characterization of ferrous sulphate hydrates. *Journal of Pharmacy and Pharmacology* **1984,** *36*, (8), 506-510. doi:https://doi.org/10.1111/j.2042-7158.1984.tb04440.x
30. Chen, D. Hygroscopicity of Pharmaceutical Crystals. Ph.D. thesis, University of Minnesota, Minneapolis, MN, USA, 2009.
31. Al-Abadleh, H. A.; Rana, M. S.; Mohammed, W.; Guzman, M. I., Dark Iron-Catalyzed Reactions in Acidic and Viscous Aerosol Systems Efficiently Form Secondary Brown Carbon. *Environ Sci Technol* **2021,** *55*, (1), 209-219. doi:10.1021/acs.est.0c05678
32. Jimenez, N. G.; Sharp, K. D.; Gramyk, T.; Ugland, D. Z.; Tran, M.-K.; Rojas, A.; Rafla, M. A.; Stewart, D.; Galloway, M. M.; Lin, P.; Laskin, A.; Cazaunau, M.; Pangui, E.; Doussin, J.-F.; De Haan, D. O., Radical-Initiated Brown Carbon Formation in Sunlit Carbonyl–Amine–Ammonium Sulfate Mixtures and Aqueous Aerosol Particles. *ACS Earth and Space Chemistry* **2022,** *6*, 228-238. doi:10.1021/acsearthspacechem.1c00395
33. Jimenez, J. L.; Canagaratna, M. R.; Donahue, N. M.; Prevot, A. S. H.; Zhang, Q.; Kroll, J. H.; DeCarlo, P. F.; Allan, J. D.; Coe, H.; Ng, N. L.; Aiken, A. C.; Docherty, K. S.; Ulbrich, I. M.; Grieshop, A. P.; Robinson, A. L.; Duplissy, J.; Smith, J. D.; Wilson, K. R.; Lanz, V. A.; Hueglin, C.; Sun, Y. L.; Tian, J.; Laadsonen, A.; Raatikainen, T.; Rautiainen, J.; Vaattovaara, P.; Ehn, M.; Kulmala, M.; Tomlinson, J. M.; Collins, D. R.; Cubison, M. J.; Dunlea, E. J.; Huffman, J. A.; Onasch, T. B.; Alfarra, M. R.; Williams, P. I.; Bower, K.; Kondo, Y.; Schneider, J.; Drewnick, F.; Borrmann, S.; Weimer, S.; Demerjian, K.; Salcedo, D.; Cottrell, L.; Griffin, R.; Takami, A.; Miyoshi, T.; Hatakeyama, S.; Shimono, A.; Sun, J. Y.; Zhang, Y. M.; Dzepina, K.; Kimmel, J. R.; Sueper, D.; Jayne, J. T.; Herndon, S. C.; Trimborn, A. M.; Williams, L. R.; Wood, E. C.; Middlebrook, A. M.; Kolb, C. E.; Baltensperger, U.; Worsnop, D. R., Evolution of organic aerosols in the atmosphere. *Science* **2009,** *326*, 1525-1529. doi:10.1126/science.1180353
34. Schnitzler, E. G.; Liu, T.; Hems, R.; Abbatt, J., Emerging investigator series: Heterogeneous OH oxidation of primary brown carbon aerosol: effects of relative humidity and volatility. *Environmental Science: Processes & Impacts* **2020**, *22*, 2162-2171. doi:10.1039/D0EM00311E
35. Zeng, L.; Dibb, J.; Scheuer, E.; Katich, J. M.; Schwarz, J. P.; Bourgeois, I.; Peischl, J.; Ryerson, T.; Warneke, C.; Perring, A. E.; Diskin, G. S.; DiGangi, J. P.; Nowak, J. B.; Moore, R. H.; Wiggins, E. B.; Pagonis, D.; Guo, H.; Campuzano-Jost, P.; Jimenez, J. L.; Xu, L.; Weber, R. J., Characteristics and evolution of brown carbon in western United States wildfires. *Atmos. Chem. Phys.* **2022,** *22*, (12), 8009-8036. doi:10.5194/acp-22-8009-2022
36. Perron, M. M. G.; Meyerink, S.; Corkill, M.; Strzelec, M.; Proemse, B. C.; Gault-Ringold, M.; Sanz Rodriguez, E.; Chase, Z.; Bowie, A. R., Trace elements and nutrients in wildfire plumes to the southeast of Australia. *Atmos. Res.* **2022,** *270*, 106084. doi:https://doi.org/10.1016/j.atmosres.2022.106084

37. Ito, A., Atmospheric Processing of Combustion Aerosols as a Source of Bioavailable Iron. *Environ. Sci. Technol. Lett.* **2015,** *2*, (3), 70-75. doi:10.1021/acs.estlett.5b00007
38. Baldo, C.; Ito, A.; Krom, M. D.; Li, W.; Jones, T.; Drake, N.; Ignatyev, K.; Davidson, N.; Shi, Z., Iron from coal combustion particles dissolves much faster than mineral dust under simulated atmospheric acidic conditions. *Atmos. Chem. Phys.* **2022,** *22*, (9), 6045-6066. doi:10.5194/acp-22-6045-2022
39. Xu, L.; Zhi, M.; Liu, X.; Gao, H.; Yao, X.; Yuan, Q.; Fu, P.; Li, W., Direct evidence of pyrogenic aerosol iron by intrusions of continental polluted air into the Eastern China Seas. *Atmos. Res.* **2023,** *292*, 106839. doi:https://doi.org/10.1016/j.atmosres.2023.106839
40. Kroll, J. H.; Donahue, N. M.; Jimenez, J. L.; Kessler, S. H.; Canagaratna, M. R.; Wilson, K. R.; Altieri, K. E.; Mazzoleni, L. R.; Wozniak, A. S.; Bluhm, H.; Mysak, E. R.; Smith, J. D.; Kolb, C. E.; Worsnop, D. R., Carbon oxidation state as a metric for describing the chemistry of atmospheric organic aerosol. *Nature Chemistry* **2011,** *3*, (2), 133-139. doi:10.1038/nchem.948

TOC artwork